Exponential decay of chaotically advected passive scalars in the zero diffusivity limit

Yue-Kin Tsang*
Institute for Research in Electronics and Applied Physics, and Department of Physics, University of Maryland, College Park, Maryland 20742, USA

Thomas M. Antonsen, Jr. and Edward Ott
Institute for Research in Electronics and Applied Physics, Department of Physics, and Department of Electrical and Computer Engineering, University of Maryland, College Park, Maryland 20742, USA
(Received 6 January 2005; published 1 June 2005)

The time asymptotic decay of the variance of a passive scalar in a chaotic flow is studied. Two mechanisms for this decay, which involve processes at short and long length scales, respectively, are considered. The validity of the short length scale mechanism, which is based on Lagrangian stretching theory, is discussed. We also investigate the regimes of applicability and observable signatures of the two mechanisms. Supporting evidence is provided by high resolution numerical experiments.

DOI: 10.1103/PhysRevE.71.066301 PACS number(s): 47.10.+g, 47.52.+j

I. INTRODUCTION AND BACKGROUND

There has been much recent interest in the problem of passive scalar advection in chaotic fluid flows. In particular, much interest has focused on the time asymptotic decay of the variance of a passive scalar [1–15]. Different mechanisms for this decay have been proposed and discussed [2,6–12,15]. It is the purpose of the present paper to investigate the validity and regimes of applicability of two of these mechanisms, one in which the damping is determined by processes occurring at short length scales [2], and one in which the damping is determined by processes taking place at the longest possible scale [6,7,11,12] (i.e., that determined by the spatial extent of the fluid itself). We note that the validity of the short length scale mechanism has been questioned [8,12,15]. In the rest of this section we provide further introductory background and discussion, and then summarize the organization of the paper.

A. The damping rate of passive scalar variance in the strange eigenfunction regime

We consider a passive scalar field subjected simultaneously to diffusion and to advection by a spatially smooth, mono-scale, fully chaotic flow in the absence of both sources and sinks of the scalar. Denoting the scalar field by $\phi(\mathbf{x},t)$, the fluid velocity field by $\mathbf{v}(\mathbf{x},t)$ (assumed incompressible), and the molecular diffusion coefficient by κ, we have that $\phi(\mathbf{x},t)$ obeys the advection-diffusion equation,

$$\partial\phi/\partial t + \mathbf{v}\cdot\nabla\phi = \kappa\nabla^2\phi, \tag{1}$$

and the initial field $\phi(\mathbf{x},0)$ is specified. In what follows we shall be interested in the case of small κ. For simplicity, we will henceforth restrict attention to the case of two-dimensional flows $\mathbf{v}(\mathbf{x},t)=[v_x(x,y,t),v_y(x,y,t)]$, and we will take the spatial average of ϕ to be zero, $\int\phi(\mathbf{x},t)d\mathbf{x}=0$.

As shown in the paper by Pierrehumbert [1] and other subsequent studies [2,5–7,11–15], for sufficiently long time this situation results in a "strange eigenfunction" in which the scalar variance decays exponentially in time [variance $\sim\exp(-\gamma(\kappa)t)$]. Furthermore, *the rate of this exponential decay $\gamma(\kappa)$ becomes independent of the diffusion coefficient κ as the diffusion becomes small*,

$$\lim_{\kappa\to 0^+}\gamma(\kappa)\equiv\gamma_0>0, \tag{2}$$

and depends only on properties of the flow.

The quantity γ_0 is the focus of the present paper. Two very different types of physical mechanisms have been advanced as possible candidates determining γ_0. We refer to these mechanisms as being either a "short wavelength mechanism" or a "long wavelength mechanism." Our main point in this paper is that both types of mechanisms are valid in the sense that there are regimes where one applies, and there are other regimes where the other applies. (These two mechanisms are not the only possible cases, as variance damping whose rate is determined by the presence of Kolmogorov–Arnold–Moser surfaces [9], or by the presence of impenetrable boundaries [10] has also been studied. These are fundamentally different from the two types of mechanism we consider here in that they do not satisfy Eq. (2), i.e., at small κ the damping due to these mechanisms approaches zero with κ.)

B. The short wavelength mechanism

1. Lagrangian stretching theory

The short wavelength mechanism is based on the use of Lagrangian stretching theory applied to rapidly varying (i.e., large wave number) components of the passive scalar field. As explained in Refs. [2,16], if one considers the passive scalar distribution to be broken up into a linear combination of "wave packet" components such that each wave packet i is localized about a point $\mathbf{x}_i(t)$, has a dominant wave number

*Present address: Courant Institute of Mathematical Sciences, New York University, New York, New York 10012.

$\mathbf{k}_i(t)$, and has a total variance $\sigma_i(t)$ [integral of the square of the scalar over the wave packet], then $\mathbf{x}_i(t)$, $\mathbf{k}_i(t)$, and $\sigma_i(t)$ evolve according to the equations

$$d\mathbf{k}_i/dt = -\mathbf{k}\cdot[\nabla\mathbf{v}(\mathbf{x},t)]_{\mathbf{x}=\mathbf{x}_i(t)}, \tag{3}$$

$$d\mathbf{x}_i/dt = \mathbf{v}(\mathbf{x}_i,t), \tag{4}$$

$$d\sigma_i/dt = -2k_i^2\kappa\sigma_i. \tag{5}$$

We note that Eqs. (3)–(5) presuppose that the smallest dimension ℓ_w and the largest dimension ℓ_ℓ characterizing the wave packet satisfy

$$k\ell_w \gg 1, \quad \ell_\ell \ll L_f, \tag{6}$$

where L_f denotes the scale length over which the smooth velocity field $\mathbf{v}(\mathbf{x},t)$ varies. The latter requirement is necessary for the validity of the local linear straining approximation, Eq. (3). Note, also, that, due to the orthogonality of sinusoids of different wave numbers, we can allow wave packets of different wave numbers to overlap spatially, and this does not spoil the result that the total variance $\Sigma(t)$ due to many wave packets is simply the sum of their individual variances,

$$\Sigma(t) = \sum_i \sigma_i(t). \tag{7}$$

Thus we can consider fields that are not locally sinusoidal with a single well-defined wavenumber at each point in space. In particular to apply Eqs. (3)–(7) to the short wavelength components of an arbitrary initial condition, $\phi_0(\mathbf{x}) = \Sigma_{\mathbf{k}} A_{\mathbf{k}} \exp(i\mathbf{k}\cdot\mathbf{x})$, one can use linearity to break each initial Fourier component, $A_{\mathbf{k}}\exp(i\mathbf{k}\cdot\mathbf{x})$, into wave packets, apply Eqs. (3)–(5), and evoke Eq. (7) (which comes from Fourier orthogonality) to superpose variances from different wave packets including those derived from different $\mathbf{k}$ components of the initial Fourier series decomposition. Note that wave packets constructed from different initial wave number components overlap spatially.

2. Finite time Lyapunov exponents

At time t_1 we consider two points $\mathbf{x}=\mathbf{y}$ and $\mathbf{x}=\mathbf{y}+\boldsymbol{\delta}_0$, that are separated by an infinitesimal displacement vector $\boldsymbol{\delta}_0$. As time t' increases from t_1 to t_2, the evolution of the displacement $\boldsymbol{\delta}(t')$ obeys the equation,

$$d\boldsymbol{\delta}/dt' = [\nabla\mathbf{v}(\mathbf{x},t')]\cdot\boldsymbol{\delta}, \tag{8}$$

where $\mathbf{x}$ is evaluated following the trajectory $\mathbf{x}(t')$ obtained from the solution of Eq. (4) with the initial condition $\mathbf{x}(t_1)=\mathbf{y}$, and the initial condition for Eq. (8) is $\boldsymbol{\delta}(t_1)=\boldsymbol{\delta}_0$. We define the (maximum) finite time Lyapunov exponent as

$$h(\mathbf{y},t_2,t_1) = \max_{\boldsymbol{\delta}_0}\left\{\frac{1}{t_2-t_1}\ln[|\boldsymbol{\delta}(t_2)|/|\boldsymbol{\delta}_0|]\right\}, \tag{9}$$

where the maximum is taken over all orientations of the infinitesimal displacement vector $\boldsymbol{\delta}_0$. Thus, for $\boldsymbol{\delta}_0$ along the direction of maximum stretching, the displacement experiences an average exponential increase of $\exp[(t_2-t_1)h]$. Since the flow is incompressible, there is also an orientation of $\boldsymbol{\delta}_0$ along which displacements decrease exponentially as $\exp[-(t_2-t_1)h]$. We now imagine that we choose $\mathbf{y}$ randomly with uniform probability density per unit area in the spatial domain of the flow. For such a random choice, h will have a probability distribution. Letting $t=t_2-t_1$, and ignoring the explicit dependence of the probability distribution on t_1, we denote this probability distribution function $P(h,t)$. For chaotic flows, large deviation theory [17–20] implies that $P(h,t)$ obeys the large t asymptotic relation, $\ln P(h,t) = -tG(h) + o(t)$, which we represent as

$$P(h,t) \sim \exp[-tG(h)]. \tag{10}$$

$G(h)$ is concave-up, $G''(h)\geq 0$, and its minimum value is defined to be zero. We denote the value of h that yields this minimum $\overline{h}$. As t becomes large Eq. (10) shows that $P(h,t)$ becomes more and more sharply peaked at $h=\overline{h}$, approaching a delta function in the limit $t\to+\infty$. Thus, as discussed in greater detail elsewhere (e.g., [20]), for all initial conditions $\mathbf{y}$ in the flow domain, except for a set of $\mathbf{y}$ of Lebesgue measure zero, the maximum Lyapunov exponent $h(\mathbf{y},t_2,t_1)$ approaches $\overline{h}$ as $t=(t_2-t_1)$ approaches infinity.

Comparing Eq. (8) and Eq. (3), Refs. [2,16] notes that, for sufficiently large time, the evolution of $|\mathbf{k}(t)|$ from an initial time $t=0$ will be approximately given by

$$|\mathbf{k}(t)| \cong |\mathbf{k}(0)|\cos\phi\exp(ht). \tag{11}$$

Here ϕ is the angle between $\mathbf{k}(0)$ and the infinitesimal displacement $\boldsymbol{\delta}_0$ along which, over the time interval 0 to t, the chaotic flow is maximally contracting when following the fluid trajectory $\mathbf{x}(t)$ originating at $\mathbf{x}(0)$.

Based on Eqs. (3)–(11), Refs. [2,16] present a mechanism leading to an exponential damping of variance in the limit [Eq. (2)] of zero diffusivity. Their result for γ_0 is

$$\gamma_0 = \min_{h\geq 0}[G(h)+h]. \tag{12}$$

We will obtain this result by another method in Sec. II. For now, the important point is that, as required for the use of Lagrangian stretching theory, Eqs. (3)–(11), the damping rate Eq. (12) is determined by processes taking place at short wavelength, $kL_f \gg 1$.

C. Long wavelength mechanisms

It was pointed out in Refs. [6,7,12] that the decay rate might also be determined by processes taking place at the largest possible passive scalar scale size determined by the extent of the fluid flow domain L_D. In these references it was shown that, for the models they considered, an analysis could be done that essentially showed that variance in the longest wavelength Fourier component dynamically exchanges variance with shorter wavelength components, leading to a net rate of transfer of variance out of the longest wavelength Fourier component. That is, one can crudely view variance as "leaking out" of the longest wavelength Fourier component and then being transferred to successively shorter wave-

length components until diffusive damping sets in. In this way the $\kappa \to 0$ decay rate γ_0 is set by the net rate of transfer out of the longest wavelength component of the strange eigenfunction.

In addition, Ref. [11] reports experimental results producing a decay rate substantially smaller than that given by Eq. (12). In this experiment the flow was produced by the Lorentz force due to electrical current flowing through the fluid in the presence of magnetic fields produced by many ($\sim$100) small magnets adjacent to the fluid container. Thus the length scale L_f of the flow velocity was determined by the distance between magnets and L_f was substantially less than the spatial extent L_D of the flow ($L_D \sim 10 L_f$). In this case the authors were able to explain their result on the basis of an effective chaotic diffusion. That is, since the flow velocity at points separated by more than L_f can be assumed to become uncorrelated, the authors of Ref. [11] view the motion of a fluid element to be similar to a random walk. Transport on the scale $L_D \gg L_f$ is thus effectively diffusive. Denoting this effective diffusion coefficient by κ_{eff}, the decay rate is dominated by the Fourier mode of longest wavelength ($\sim L_D$),

$$\gamma_0 \sim \kappa_{\text{eff}}/L_D^2. \tag{13}$$

Note that γ_0 in Eq. (13) can be made arbitrarily small if one allows L_D to become large keeping L_f fixed.

D. Validity of Lagrangian stretching theory

References [8,15] present an argument showing that the Lagrangian stretching theory description of the evolution of the distribution of a passive scalar eventually breaks down if sufficiently long time intervals are considered. Based on this result, the validity of Eq. (12) has been questioned. In order to discuss this issue further, we now briefly review the argument.

Consider the passive scalar density $\phi(\mathbf{y},t)$ at a fixed point $\mathbf{y}$ and at a time t. We now ask, if we give the passive scalar field, $\phi(\mathbf{x},t-\tau)$, at a previous time $t-\tau$, $\tau > 0$, which region of $\mathbf{x}$-space contributes to determining the passive scalar density, $\phi(\mathbf{y},t)$, at point $\mathbf{y}$ and time t? This can be determined by backward integration of Eq. (1) from time t to time $t-\tau$. For sufficiently small τ chaotic advective spreading is unimportant and diffusion dominates, giving a region of influence,

$$|\mathbf{x}-\mathbf{y}_\tau|^2 \lesssim \kappa\tau, \tag{14}$$

where $\mathbf{y}_\tau$ denotes the location at time $t-\tau$ that is advected to $\mathbf{y}$ at time t. When $|\mathbf{x}-\mathbf{y}_\tau|$ becomes sufficiently large, the chaotic advective spreading becomes faster than the diffusive spreading. This occurs when

$$|\mathbf{x}-\mathbf{y}_\tau|^2 \overline{h} \gtrsim \kappa, \tag{15}$$

where $\overline{h}$ denotes the infinite time Lyapunov exponent here taken to represent a typical stretching rate. From Eq. (14) and Eq. (15) the crossover between the spreading being diffusion-dominated and the advection-dominated occurs when

$$\tau \sim \tau' \equiv 1/\overline{h}, \tag{16}$$

at which time the region of influence is

$$|\mathbf{x}-\mathbf{y}_\tau| \lesssim \sqrt{\kappa/\overline{h}}. \tag{17}$$

For τ larger than τ', the region of influence initially expands exponentially along the backward-expanding direction (due to the chaotic advection), and maintains its width at $(\kappa/\overline{h})^{1/2}$ (due to a balance of diffusion and contraction). Thus the region of influence becomes a very long, thin filament with a length

$$\ell(\tau) \sim \sqrt{\kappa/\overline{h}}\exp[\tau\overline{h}], \tag{18}$$

where we have neglected τ' compared to τ. As time proceeds, $\ell(\tau)$ becomes of order L_f and then begins to bend and fold. Eventually, because of its nonzero width ($\sim\sqrt{\kappa/\overline{h}}$) the filament "packs" [8] the flow domain. Assuming $L_D = L_f$, this occurs when the filament area, $(\kappa/\overline{h})^{1/2}\ell(\tau)$, is equal to the area of the flow domain, L_f^2, or [15],

$$\tau'' \sim \overline{h}^{-1}\ln[L_f^2\overline{h}/\kappa]. \tag{19}$$

At this time, different segments along the filament start merging together, and the exponentially decaying strange eigenfunction becomes established. Since the process of folding and the resulting packing and filament merging is absent in the Lagrangian stretching theory, its validity may be expected to be restricted to time intervals that do not exceed τ''.

Since it may be expected that the regime of exponentially decaying variance is only established over a sufficiently long time $t \gg \tau''$, and since the exponential decay, in principal, lasts forever, the validity of Eq. (12), which has been derived by use of Lagrangian stretching theory, valid only for time intervals less than τ'', has been questioned. Several papers have recently noted the uncertain state of affairs in this regard [8,13–15,21]. In contrast, in Sec. II we show that Eq. (12) is indeed valid under appropriate conditions. The basic reasoning is as follows. Imagine that a sufficient time has passed that a strange eigenfunction with exponentially decaying variance has been established. Now, *starting at this time*, we can use Lagrangian stretching theory to advance the short wavelength components of the spectrum forward in time and obtain the short wavelength mechanism damping rate [i.e., Eq. (12)]. Note that to do this we only need to evolve the passive scalar field for a relatively short time (e.g., of the order of γ_0^{-1}), and are not required to leave the range of validity of the Lagrangian theory set by τ''.

As we note later in the paper, even in the absence of a prediction for the damping rate from Eq. (12), there is still a clear distinction that could potentially be experimentally drawn between the two mechanisms. Namely, for small κ, the long wavelength mechanism produces a wave number power spectrum that *decreases* with increasing wave number as a power law, while the short wavelength mechanism produces a wave number power spectrum that is essentially flat out to the diffusively-determined cutoff range.

E. Outline

In Sec. II we (i) present a theoretical argument that, subject to the satisfaction of a certain hypothesis, the zero diffusivity damping rate γ_0 can never exceed the damping rate Eq. (12) determined by the short wavelength mechanism; (ii) discuss the distinct wave number power spectrum signatures of the two mechanisms we consider; and (iii) introduce the technique that we will subsequently apply in Sec. IV for numerical evaluation of the theoretical predictions of the short wavelength mechanism damping rate [Eq. (12)] and of the theoretical prediction of the long wavelength mechanism's power-law wave number power spectrum decay exponent. In Sec. III we (i) introduce the flow that we will use for our numerical experiments; (ii) show that the flow satisfies the hypothesis used in Sec. II in the derivation of the upper bound on γ_0; and (iii) obtain another upper bound on γ_0 for this flow. In Sec. IV we present our numerical experiments including the following: (i) computations of the damping rate for system sizes up to 6×10^4 by 6×10^4 grid points; (ii) computations of wave number power spectra; (iii) introduction of a spatial filtering technique designed to numerically distinguish the applicability of the long and short wavelength mechanisms; and (iv) consideration of a range of values of (L_D/L_f) thereby obtaining situations at low values (L_D/L_f) where the short wavelength mechanism apparently applies, and others at higher values of (L_D/L_f) where the long wavelength mechanism apparently applies. Section V concludes the paper. The main contributions of this paper are (i) the provision of a justification for the applicability of two mechanisms [one of which, Eq. (12), has been previously questioned] leading to a positive exponential damping rate of scalar variance in the $\kappa\to0^+$ limit [i.e., Eq. (2)]; (ii) a discussion of the respective regimes of applicability of and observable signatures of the two mechanisms; and (iii) supporting evidence of numerical experiments at much higher numerical resolution than previously employed.

II. THE EXPONENTIAL DAMPING RATE AND THE FORM OF THE STEADY STATE WAVE NUMBER POWER SPECTRUM

A. Upper bound on the zero diffusivity damping rate

We begin by assuming a situation where a long wavelength mechanism determines the time-asymptotic exponential decay rate of a strange eigenfunction. For wave numbers $k\ll k_d\equiv(\overline{h}/\kappa)^{1/2}$ diffusion can be neglected [2] [compare with Eq. (17)]. Since we are interested in the limit of diffusivity approaching zero, we can consider a range of wave numbers,

$$k_d=(\overline{h}/\kappa)^{1/2}\gg k\gg k_f=2\pi/L_f. \tag{20}$$

In this range we can use diffusionless local stretching theory to evolve the k spectrum forward in time, provided that k does not become too small $(k\sim k_f)$ or too large $(k\sim k_d)$ over the finite time interval that we consider for the evolution. For any time interval, we can always find a range of k where this is satisfied, since we can consider arbitrarily small values of κ. Denote the spectrum ensemble averaged over random flow realizations at time t_0 by $S_0(k)$. Then, using Eq. (11) and assuming we are in the time asymptotic exponential decay regime, the spectrum at a later time t_0+t is

$$S_0(k)\exp(-\gamma_0 t)=\int_0^\infty dhP(h,t)\int_0^{2\pi}\frac{d\phi}{2\pi}\int dk'S_0(k')\times\delta[k-k'(e^{2ht}\cos^2\phi+e^{-2ht}\sin^2\phi)^{1/2}], \tag{21}$$

where, for simplicity, we have taken S_0 to be isotropic (we return to this assumption shortly). In Eq. (21) the cos ϕ term and the sin ϕ term are respectively due to the components of the initial wave vector along the contracting and expanding directions. We want to show that the evolution Eq. (21) can be satisfied for $S_0>0$ only if $\gamma_0<\min_{h\geqslant0}\{G(h)+h\}$ applies. In order to match the k dependence on the two sides of Eq. (21), $S_0(k)\sim k^{-\psi}$ in the range of k considered. Thus we obtain

$$\exp(-\gamma_0 t)=\int_0^\infty dhP(h,t)\int_0^{2\pi}\frac{d\phi}{2\pi}(e^{2ht}\cos^2\phi+e^{-2ht}\sin^2\phi)^{-(1-\psi)/2}. \tag{22}$$

For large time, $ht\gg1$, the integral over ϕ yields

$$\int_0^{2\pi}d\phi(e^{2ht}\cos^2\phi+e^{-2ht}\sin^2\phi)^{-(1-\psi)/2}\sim e^{-(1-|\psi|)ht}, \tag{23}$$

for $\psi\neq0$. From Eq. (22) we then have

$$\exp(-\gamma_0 t)\sim\int_0^\infty P(h,t)e^{-(1-|\psi|)ht}dh. \tag{24}$$

Using Eq. (10) for $P(h,t)$ and letting t be large, this gives

$$\gamma_0=\min_{h\geqslant0}\{G(h)+h-|\psi|h\}. \tag{25}$$

Thus,

$$\gamma_0<\min_{h\geqslant0}\{G(h)+h\}, \tag{26}$$

which is what we wanted to show.

Now we consider our assumption of isotropic S_0. In general, of course, the spectrum will depend on the orientation of the wave vector $\mathbf{k}$ (i.e., it is nonisotropic). To proceed we adopt the hypothesis that, as a function of the orientation of $\mathbf{k}$, we can bound S_0 above and below, as follows:

$$Ak^{-\psi}>S_0(\mathbf{k})>Bk^{-\psi}, \tag{27}$$

where A and B are finite and positive. The validity of this hypothesis is not to be taken for granted. For the case of the flow treated in the next section, we will show that Eq. (27), in fact, is satisfied. For another case, treated in Ref. [12], it appears that Eq. (27) may be violated (this has been discussed in [12]). Assuming Eq. (27) and proceeding as above, Eqs. (21)–(24), we obtain

$$\frac{A}{B}I>\exp(-\gamma_0 t)>\frac{B}{A}I, \tag{28}$$

where I is the integral on the right hand side of Eq. (22). For large t, Eq. (28) again yields Eq. (26).

According to Eq. (26), if a long wavelength mechanism determines the damping and if hypothesis Eq. (27) is satisfied, then, by comparison of Eq. (25) and Eq. (12), γ_0 must be less than the damping rate determined by the short wavelength mechanism, Eq. (12). Since these mechanisms are determined in opposite ranges of the k-spectrum there is no *a priori* reason that γ_0 determined by long wavelength processes should always be less than γ_0 determined by short wavelength processes [Eq. (12)], or vice versa. We conclude on this basis that it is reasonable to suspect that either mechanisms may apply, depending on the configuration of the flow. That is, subject to the satisfaction of hypothesis Eq. (27), the short wavelength result Eq. (12) is applicable if long wavelength considerations yield a damping rate that exceeds Eq. (12). In Sec. IV, we present numerical evidence that this is indeed the case.

To close this subsection we note the special role of the variance ($\Sigma(t)=\int \phi^2 d\mathbf{x}$) as opposed to higher moments of the scalar ($\Sigma_p(t)=\int \phi^{2p} d\mathbf{x}, p=2,3,\ldots$). In particular, our derivation above relies on Eq. (7) holding even when wave packets with well-defined wave numbers $\mathbf{k}_i$ overlap spatially. The validity of Eq. (7) in this case is a consequence of the orthogonality of Fourier modes. A relation like Eq. (7) does not apply for higher moments, and thus predictions for the exponential damping rate of $\Sigma_p(t)$ as given in Refs. [3,4] do not apply to the time asymptotic, strange eigenfunction regime (see discussion in Refs. [8,15]).

B. Wave number power spectrum

We now invert Eq. (25) to obtain the spectral exponent ψ in terms of γ_0 and $G(h)$. Rewriting the result for γ_0 we have

$$\min_{h\geq 0}\{G(h)+h-|\psi|h-\gamma_0\}=0. \tag{29}$$

Since the function in the curly bracket has a minimum of zero, it is non-negative. Thus multiplying it by any positive function of h again produces a positive function of h whose minimum is zero. Multiplying by $1/h$ we obtain

$$\min_{h\geq 0}\{h^{-1}[G(h)-\gamma_0]+1-|\psi|\}=0. \tag{30}$$

This gives the spectral exponent for the power-law decay of S_0 with k,

$$\psi=\pm\left[1+\min_{h\geq 0}\left\{\frac{G(h)-\gamma_0}{h}\right\}\right]. \tag{31}$$

Since the scalar spectrum propagates from low wave number to high wave number and is dissipated at high wave number, it seems physically unreasonable that $\psi<0$ [i.e., $S(k)$ increases algebraically with k]. Thus we reject the negative solution in Eq. (31). This is consistent with our numerical results as well as previous studies of the long wavelength mechanism [6,7,11–13]. Equation (31) (with the plus sign) also appears in Ref. [15] by Fereday and Haynes. Similar results have previously been given for problems involving the convection of vector (rather than scalar) fields: Ref. [22] does this for the kinematic dynamo problem (in which case the relevant convected field is the magnetic field), while Ref. [23] applies to the problem of the stability of a smooth Lagrangian chaotic fluid flow [in which case the relevant convected field is the fluid vorticity $\boldsymbol{\omega}(\mathbf{x},t)=\nabla\times\mathbf{v}(\mathbf{x},t)$].

Although Eq. (31) was derived under the assumption that Eq. (26) holds (i.e., a long wavelength mechanism is operative), we note that, when the short wavelength result Eq. (12) is substituted in Eq. (29), we obtain $\psi=0$, and, as γ_0 increases from zero to the value given by Eq. (12), the exponent ψ decreases from one to zero. This suggests that long and short wavelength mechanisms should be distinguishable via examination of the wave number power spectrum of the passive scalar in the time-asymptotic, strange eigenfunction regime. In particular, log-log plots for spectra corresponding to the short wavelength mechanism should be essentially flat out to k of order k_d, while similar plots corresponding to a long wavelength mechanism should decrease linearly with the logarithm of k. Numerical evidence supporting this will be provided in Sec. IV.

C. Numerical technique for evaluating γ_0 from Eq. (12) and ψ from Eq. (31)

Equation (12) gives the short wavelength mechanism γ_0 as the minimum of $[G(h)+h]$ over h, and Eq. (31) gives the long wavelength mechanism ψ as one plus the minimum of $\{h^{-1}[G(h)-\gamma_0]\}$ over h. One method of computing these quantities, employed in Ref. [2], is to first obtain a numerical estimate of $G(h)$ and then to perform the minimization. The computation of numerical approximations to $G(h)$ for flows of the type we examine has been previously performed in Refs. [2,19]. The technique employed was to first compute histogram approximations to $P(h,t)$ using a large number (N) of uniformly distributed initial conditions $\mathbf{y}_i$ ($i=1,2,\ldots,N$) to compute many values of $h_i(t)\equiv h(\mathbf{y}_i,t_2,t_1)$, $t\equiv t_2-t_1$ from Eq. (9). Approximations to $G(h)$ were then computed from plots of $t^{-1}\ln[P(h,t)]+C$, where C was adjusted so that the minimum of the numerical estimate of $G(h)$ was zero. By varying N and t, the convergence and accuracy of these estimates could be crudely judged.

In this paper we use an alternate numerical method for evaluating the short wavelength mechanism γ_0 and the long wavelength mechanism ψ. This alternate method has been previously used to numerically calculate similar quantities in Refs. [23,24]. The alternate method, which circumvents the need for obtaining a numerical estimate of $G(h)$, is simpler to implement and is found to be more accurate and better convergent.

To illustrate the method we first consider the problem of finding the minimum of $[G(h)+h]$ (i.e., of finding the prediction of the value of γ_0 due to the short wavelength mechanism). Noting from Eq. (10) that the average of $\exp(-ht)$ over many initial conditions is

$$\langle\exp(-ht)\rangle=\int P(h,t)e^{-ht}dh\sim\exp\{-\min_{h\geq 0}[G(h)+h]t\}, \tag{32}$$

we employ the following procedure. As before, we first compute many values of $h_i(t)$. Then we estimate $\langle\exp(-ht)\rangle$ as

$$\langle \exp(-ht)\rangle_N = N^{-1}\sum_{i=1}^{N} \exp[-h_i(t)t], \tag{33}$$

plot $\ln\langle\exp(-ht)\rangle_N^{-1}$ versus t, and finally estimate $\min_{h\geqslant 0}[G(h)+h]$ as the slope of this curve. We note that it is important to ensure that N is large enough. In particular,

$$\min_{h\geqslant 0}[G(h)+h] < \overline{h}, \tag{34}$$

but as $t\to\infty$, with N fixed, Eq. (33) will always approach $\exp(-\overline{h}t)$, erroneously yielding the estimate $\overline{h}$. This is because, as mentioned in Sec. I B 2, in the $t\to\infty$ limit, $h_i(t)\to\overline{h}$ for almost every initial condition $\mathbf{y}_i$ (except for a set of $\mathbf{y}$ of Lebesgue measure zero). Thus N must be made larger as t is increased. The point is that, with increasing t, the average Eq. (33) is dominated by a smaller and smaller fraction of initial conditions i for which $\exp[-h_i(t)t]$ is much bigger than its value for the vast majority of other initial conditions (e.g., see Ref. [20]). This same problem is also present when applying the method based on estimation of $G(h)$ from histograms, but we have found that the alternate method based on Eq. (33) appears to converge significantly quicker in t, and so this problem is less severe.

Similar considerations can be applied to compute ψ from Eq. (29). As done for Eq. (12), a result analogous to Eq. (32) is

$$\langle \exp[-(1-\psi)ht]\rangle \sim \exp\{-\min_{h\geqslant 0}[G(h)+(1-\psi)h]t\}. \tag{35}$$

Thus, for fixed ψ $(1>\psi>0)$, the large t slope of a plot of $\ln\{\langle\exp[-(1-\psi)ht]\rangle\}^{-1}$ versus $\ln t$ provides an estimate of γ_0 for the long wavelength mechanism. Varying ψ we construct a plot of γ_0 versus ψ, from which, given the damping rate γ_0, the spectral power-law exponent ψ is obtained.

III. THE MODEL FLOW

A. Specification of the velocity field

Our numerical experiments in Sec. IV will be performed using the following prescribed velocity field [1,2],

$$\mathbf{v}(\mathbf{x},t) = U\{\mathbf{x}_0 f(t)\cos[(2\pi y/L_f)+\theta_1(t)] + \mathbf{y}_0[1-f(t)]\cos[(2\pi x/L_f)+\theta_2(t)]\}. \tag{36}$$

Here the time dependent functions $f(t)$, $\theta_1(t)$ and $\theta_2(t)$ are defined as follows:

$$f(t) = \begin{cases} 1 & \text{for } nT\leqslant t<(n+1/2)T, \\ 0 & \text{otherwise,} \end{cases} \tag{37}$$

$$\theta_1(t) = \alpha_n \text{ for } nT\leqslant t<(n+1/2)T, \tag{38}$$

$$\theta_2(t) = \beta_n \text{ for } (n+1/2)T\leqslant t\leqslant (n+1)T, \tag{39}$$

where n is an integer, and α_n and β_n are random numbers uniformly distributed in $[0,2\pi]$, uncorrelated for different n, and uncorrelated between α_n and β_n. Integrating the flow Eq. (36) over one time period T, we obtain a map expressing the position of a fluid element (x_{n+1},y_{n+1}) at time $t=(n+1)T$ in terms of its position (x_n,y_n) at time $t=nT$,

$$x_{n+1} = x_n + (UT/2)\cos[(2\pi y_n/L_f)+\alpha_n], \tag{40a}$$

$$y_{n+1} = y_n + (UT/2)\cos[(2\pi x_{n+1}/L_f)+\beta_n]. \tag{40b}$$

The flow Eq. (36) is periodic in (x,y) space with a periodicity length L_f. We take the passive scalar to be periodic with a periodicity length $L_D=ML_f$ where M is an integer. That is, the advection-diffusion equation [Eq. (1)] will be solved for $\mathbf{v}(x,y,t)$ given by Eq. (36) with periodic boundary conditions on the scalar field, $\phi(x\pm L_D,y\pm L_D)=\phi(x,y)$. We note that our choice of a random flow precludes the possibility of Kolmogorov-Arnold-Moser surfaces and ensures that fluid trajectories are chaotic and ergodic within the entire periodic cell, $0\leqslant x<L_D$, $0\leqslant y<L_D$. Furthermore, the imposed randomness of the flow simulates realistic typical situations where fluid instabilities lead to nonperiodic, temporally chaotic time dependence of the velocity field.

B. Is Eq. (27) satisfied?

We now discuss whether our specified flow configuration, Eqs. (36)–(39), will lead to a spectrum satisfying hypothesis Eq. (27). If it does, then, as shown in Sec. II, the short wavelength mechanism result Eq. (12) supplies an upper bound on the $\kappa\to 0^+$ damping rate γ_0. The key requirement in Eq. (27) is $B>0$. For the flow in Eq. (36) we note that the randomness of α_n and β_n can be used to guarantee that $B>0$. If it were zero, then the spectrum $S_0(\mathbf{k})$ would be smaller than $O(k^{-\psi})$ for some particular orientation, or range of orientations, of $\mathbf{k}$. Assume this is the case. For large k this says that in the vicinity of every point $\mathbf{x}$ in the domain the local high k spectrum is smaller than $O(k^{-\psi})$ in this direction. Now apply the map Eqs. (40) to the assumed spectrum. Each of these map applications rotates the angular range of the local high k spectrum by a random amount that is different at different points $\mathbf{x}$. After several map applications, Eqs. (40) have the property that the assumed angular range of smaller than $O(k^{-\psi})$ values of the local spectra can be rotated to any direction, and these directions are different at different $\mathbf{x}$. Thus the assumed range where $S_0(\mathbf{k})$ is smaller than $O(k^{-\psi})$ cannot be maintained and we conclude that $B>0$. We have tested this numerically using the simulations described in Sec. IV. Figure 1, corresponding to $\kappa T/L_D^2=1.09\times 10^{-9}$ (see curve with this label in Fig. 5), shows polar plots of $S(k,\varphi)$ $(k\equiv|\mathbf{k}|,\tan\varphi\equiv k_y/k_x)$ obtained for a single random realization of the flow [Eqs. (36)–(39)] at a representative instant of time. These plots are consistent with our supposition that a range of φ in which $S(k,\varphi)=0$ does not occur.

C. Upper bound on γ_0 for the flow given in Eq. (36)

In this section we find an upper bound to the decay rate of variance based on the rate at which variance is removed from the longest wavelength mode present in the scalar. Let

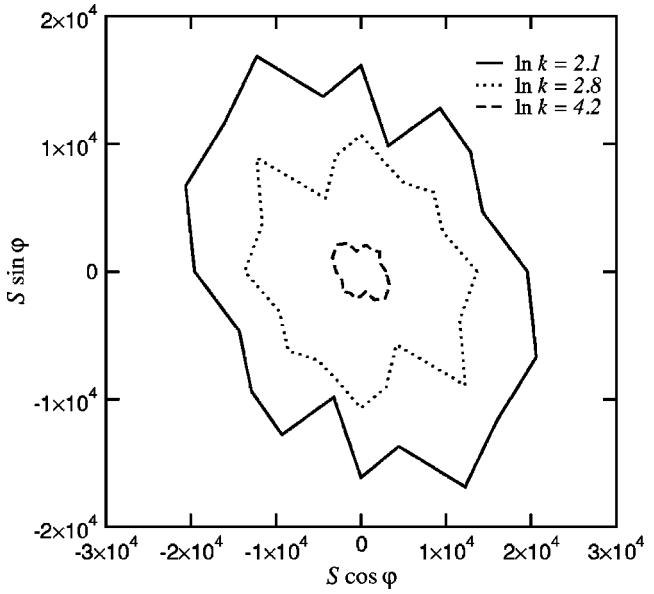

FIG. 1. Polar plot of $S(k,\varphi)$; $k\equiv|\mathbf{k}|$, $\tan\varphi\equiv k_y/k_x$. At each φ the discrete wave number spectrum $(k_x=2m\pi/L_D, k_y=2n\pi/L_D)$ is averaged over a range of $\Delta k=8$ and $\Delta\varphi=18°$. $\kappa T/L_D^2=1.09\times10^{-9}$.

$\phi_n(x,y)$ denote the passive scalar field at time $t=nT$. Evolving this field by the map Eq. (36) we have

$$\hat{\phi}_{n+1}(x,y)=\phi_n(x',y'), \tag{41}$$

where x' and y' are obtained from the inverse mapping, $y'=y-(UT/2)\cos[(2\pi x/L_f)+\beta_n]$, $x'=x-(UT/2)\times\cos[(2\pi y'/L_f)+\alpha_n]$. The transformation Eq. (41) applies in the case $\kappa=0$. Thus, it preserves the total scalar variance, redistributing variance in wave number space. We first consider the effect of Eq. (41) on a scalar which at time n consists of a single Fourier component at the lowest allowed wave number,

$$\phi_n(x,y)=A_n\sin(2\pi y/L_D), \tag{42}$$

where $L_D=ML_f$. Equation (41) then yields,

$$\hat{\phi}_{n+1}(x,y)=A_n\sin\left\{\frac{2\pi}{ML_f}\left[y-\left(\frac{UT}{2}\right)\cos\left(\frac{2\pi x}{L_f}+\beta_n\right)\right]\right\}. \tag{43}$$

This function has Fourier wave number components at $\mathbf{k}=[2\pi m/L_f, \pm2\pi/(ML_f)]$ where m is an integer. Now assume that a fictitious $\mathbf{k}$-dependent damping is applied that strongly dissipates all the Fourier components $|\mathbf{k}|>2\pi/(ML_f)$, but does not damp the Fourier component $|\mathbf{k}|=2\pi/(ML_f)$. This results in a passive scalar field, $\phi_{n+1}(x,y)=\int_0^{L_f}\hat{\phi}_{n+1}(x',y)dx'/L_f$, or

$$\phi_{n+1}(x,y)=A_nJ_0(\eta)\sin(2\pi y/L_D) \tag{44}$$

where $\eta=\pi UT/(ML_f)$ and $J_0(\eta)$ is the zeroth order Bessel function. Thus, the variance has decreased by the factor $[J_0(\eta)]^2$. Since this fictitious damping is much larger than the molecular diffusive damping used in Eq. (1) with $\kappa\to0^+$, we conclude that given Eq. (42), Eq. (44) must provide an upper bound on the $\kappa\to0^+$ damping rate,

$$\gamma_0\leqslant-\frac{1}{T}\ln[J_0(\eta)]^2. \tag{45}$$

Now, we consider the initial condition used in our numerical experiments, namely,

$$\phi_0(x,y)=A_0\sin[2\pi(x+y)/L_D]. \tag{46}$$

Because of the form of our map Eq. (36), at time $n=1$ the Fourier components excited from the initial condition Eq. (46) are $\mathbf{k}=[\pm2\pi m_x/L_f\pm2\pi/(ML_f), \pm2\pi m_y/L_f\pm2\pi/(ML_f)]$, where m_x and m_y are integers. Furthermore, subsequent applications of the map again return these same Fourier wave number components. Thus at any time n, the mode of longest possible wavelength is $\mathbf{k}=[\pm2\pi/(ML_f), \pm2\pi/(ML_f)]$ if $M\geqslant2$. Thus for $M\geqslant2$ we can proceed in a manner similar to what was done above. We evolve $\phi_n=A_n\sin[2\pi(x+y)/(ML_f)]$ by the map Eq. (36) to obtain $\hat{\phi}_{n+1}$ and then introduce a fictitious damping to dissipate all but the longest wavelength Fourier mode in $\hat{\phi}_{n+1}$. The resulting scalar field is given by

$$\phi_{n+1}(x,y)=[J_0(\eta)]^2\phi_n(x,y). \tag{47}$$

Therefore, for the initial condition Eq. (46), we have the following upper bound for γ_0,

$$\gamma_0\leqslant-\frac{1}{T}\ln[J_0(\eta)]^4. \tag{48}$$

In addition, for $\eta\ll1$ (M large), we obtain

$$\gamma_0\leqslant\frac{\eta^2}{T}=2\left(\frac{2\pi}{ML_f}\right)^2\kappa_{\text{eff}}, \tag{49}$$

where

$$\kappa_{\text{eff}}=\frac{1}{8}U^2T. \tag{50}$$

This is in agreement with the definition $\kappa_{\text{eff}}=\langle(\Delta x)^2+(\Delta y)^2\rangle/2T$ if (Δx^2) and $(\Delta y)^2$ are computed from the map Eq. (36) and the random angles α_n and β_n are averaged over. Equations (49) and (50) are also in agreement with Eq. (13). Thus while Eq. (48) is an upper bound, it approaches the true value of γ_0 as $L_D/L_f=M\to\infty$. If the upper bound Eq. (48) is lower than that provided by the short wavelength mechanism damping rate Eq. (26), then the short wavelength damping mechanism does not apply. We conclude that, for the flow given by Eqs. (36)–(39) and the initial condition Eq. (46), a sufficient condition for the applicability of a long wavelength mechanism is

$$\min_{h\geqslant0}[G(h)+h]>-\frac{1}{T}\ln[J_0(\eta)]^4. \tag{51}$$

IV. NUMERICAL EXPERIMENTS

We numerically solve the advection diffusion problem for the flow Eqs. (36)–(39) using a modification in which the

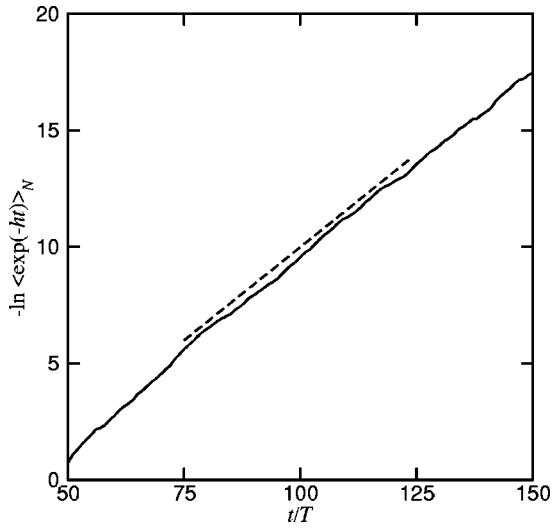

FIG. 2. Log-linear plot of $\langle \exp(-ht) \rangle_N^{-1}$ versus t. The dashed line is a linear fit whose slope gives prediction for γ_0 by the short wavelength mechanism.

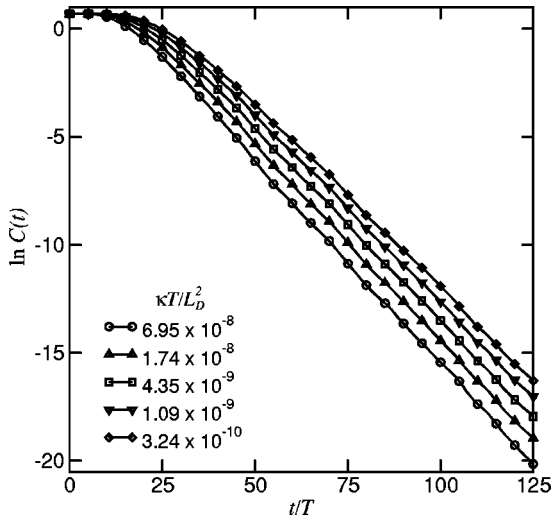

FIG. 3. Exponential decay of scalar variance with time at different diffusivity κ.

flow is applied without diffusion for each time step, $nT \leqslant t \leqslant (n+1)T$, followed by a diffusive step in which the passive scalar field is diffusively smoothed. In addition, we use the "lattice method" of Ref. [5] which employs a square grid representation of the scalar field. There are various ways of doing this. The particular implementation we use is outlined in the Appendix. The main point is that, because of the simplicity and parallelizability of this method, computations can be very fast, and the use of very high resolutions becomes feasible. For results reported in this section, the initial condition for the passive scalar is taken to be $\phi(\mathbf{x}, t=0) = 2 \sin[2\pi(x+y)/L_D]$ and we use $UT = \pi$ in Eq. (40).

Following the procedures described in Sec. II C, we calculate the theoretical value γ_0 for our flow from Eq. (12) by plotting $-\ln\langle \exp(-ht) \rangle_N$ versus t in Fig. 2, where we have considered $N = 8192^2$ initial conditions. By measuring the slope of the curve, the prediction for γ_0 by the short wavelength mechanism is estimated to be 0.16.

A. Numerical experiments with $L_D = L_f$

In this case, we will find results consistent with the hypothesis that the short wavelength mechanism applies and γ_0 is given by Eq. (12). Figure 3 shows the exponential decay of the scalar variance $C(t) = 1/L^2 \int \phi^2 d\mathbf{x}$ for different diffusivity κ (refer to the Appendix for the definition of κ in our lattice model). The decay rates $\gamma(\kappa)$ are measured and plotted in Fig. 4. As expected, $\gamma(\kappa)$ decreases with κ. At the smallest κ we achieve, which corresponds to a grid of 6×10^4 by 6×10^4, $\gamma(\kappa)$ is estimated to be 0.17, which is within 6% of the theoretical value (0.16) predicted by the short wavelength mechanism.

We have tried extrapolating our small κ results to $\kappa = 0$, but we find that the extrapolated value depends sensitively on small changes in our numerically determined $\gamma(\kappa)$ and on the assumed form of the fitting function. For example, using a three parameter (γ_0, A, B) fit of our numerical data to the fitting function $\gamma(\kappa) = \gamma_0 + A\kappa^B$, we obtain $\gamma_0 \approx 0.16$, if we determine $\gamma(\kappa)$ by fits to data in Fig. 3 restricted to the range $-20 \leqslant \ln C \leqslant -10$, but we obtain a much lower extrapolated value using data from the range $75 \leqslant t/T \leqslant 125$. This extreme sensitivity to the resulting tiny difference in $\gamma(\kappa)$ by these two determinations is indicated by the small values of the best fitted exponent B (e.g., 0.13 in the first case), corresponding to very steep decrease of $\gamma(\kappa)$ as $\kappa \to 0$. Thus, we view our computational results for $\gamma(\kappa)$ as not being definitive, and we seek other means of testing for whether the short wavelength mechanism is operative.

More definite evidence for the short wavelength mechanism is provided by examining the wavenumber power spectrum $S(k,t)$ in the strange eigenfunction regime. $S(k,t)$ is defined as

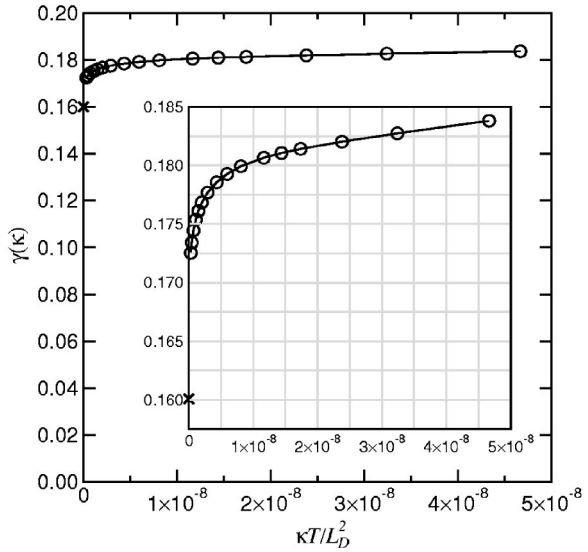

FIG. 4. Exponential decay rate of the scalar variance at different diffusivity (circle). The theoretical prediction by the short wavelength mechanism Eq. (12) is also plotted (cross). The inset plots the same data on a different scale.

$$S(k,t) = \int \frac{d\mathbf{k}'}{(2\pi)^2} \delta(k - |\mathbf{k}'|) \frac{|\tilde{\phi}(\mathbf{k}',t)|^2}{L_D^2}, \tag{52}$$

where $\tilde{\phi}(\mathbf{k},t)$ is the Fourier transform of the scalar field $\phi(\mathbf{x},t)$. In the strange eigenfunction regime, $S(k,t) \sim \exp(-\gamma_0 t)\overline{M}(k)$ [1,2]. Hence, we consider the time-averaged spectrum $S_{\text{avg}}(k)$ defined as

$$S_{\text{avg}}(k) = \langle S(k,t)/C(t) \rangle_t. \tag{53}$$

Figure 5 shows a log-log plot of $S_{\text{avg}}(k)$ versus k for different κ. These curves are obtained by time-averaging in the interval $90 \leqslant t/T \leqslant 100$. For all κ, $S_{\text{avg}}(k)$ is essentially flat out to the diffusive cutoff scale k_d (note in particular the curve for $\kappa T/L_D^2 = 1.09 \times 10^{-9}$). As explained in Sec. II, this indicates that γ_0 is determined by the short wavelength mechanism.

To obtain our strongest evidence for the applicability of the short wavelength mechanism for the case $L_D = L_f$, we introduce the following spatial filtering technique. Prior to performing the advection step and the diffusive smoothing step on every period, we remove all Fourier components $\tilde{\phi}(\mathbf{k},t)$ with $|k_x| \leqslant ak_0$ and $|k_y| \leqslant ak_0$ where $k_0 = 2\pi/L_D$ and $a > 0$. This essentially introduces a very strong long wavelength damping. Keeping ak_0/k_d fixed ($k_d \sim 1/\sqrt{\kappa}$), insensitivity of the damping rate $\gamma(\kappa)$ to a shows that mechanisms at long wavelengths do not determine the damping, and thus indicates that the short wavelength mechanism applies. We employed such long wavelength damping in our numerical experiments after the initial transient (20 periods) of the variance decay. Figure 6 shows the scalar variance as a function of time for five different pairs of κ and a, each with the same ak_0/k_d ratio. It shows clearly that at large t, all curves are more or less parallel to each other, and thus the decay rate $\gamma(\kappa)$ is approximately the same in all cases. Figure 7 plots $\gamma(\kappa)$ versus $\log_2 \sqrt{\kappa T/L_D^2}$ for different values of a. The dotted lines connect data points with the same ak_0/k_d ratio. This result is consistent with $\gamma(\kappa)$ being independent of a given a fixed ak_0/k_d and provides very strong evidence that $\gamma(\kappa)$ is determined by the short wavelength mechanism when $L_D = L_f$.

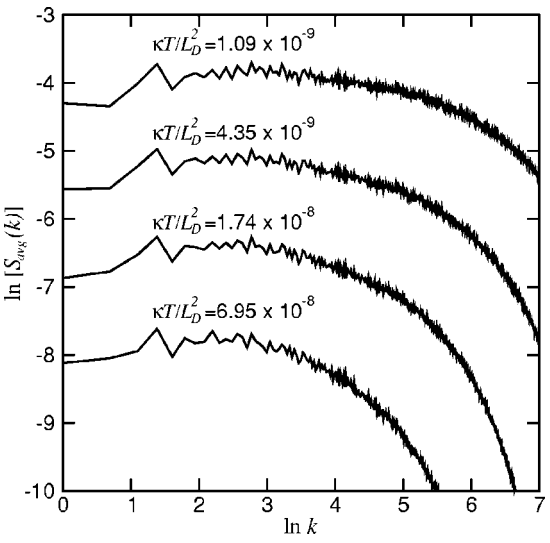

FIG. 5. Averaged wave number power spectra $S_{\text{avg}}(k)$ at different diffusivity κ.

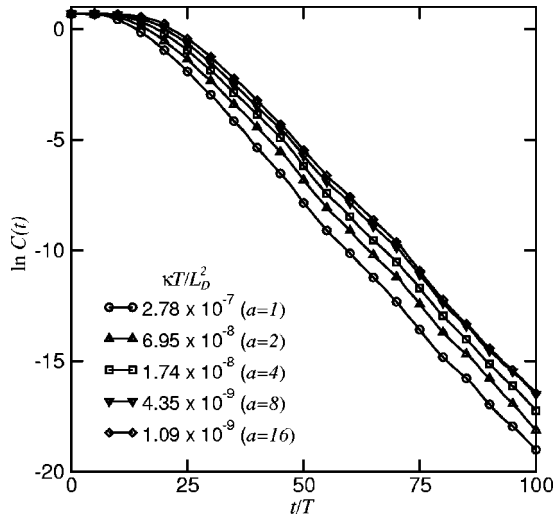

FIG. 6. Decay of scalar variance under large long wavelength damping with the ratio ak_0/k_d kept fixed.

B. Numerical experiments with $L_D > L_f$

As described in Sec. I C, the behavior of the system for the case $L_D > L_f$ can be quite different from that for $L_D = L_f$. In particular, if $L_D > L_f$, the velocity field varies on scales smaller than the longest length scale of the scalar field. When Eq. (51) is satisfied, the long wavelength mechanism must determine the variance damping rate.

Letting $L_D = ML_f$, we study the variance decay for different values of M. Figure 8 plots the damping rate $\gamma(\kappa)$ as a function of M for simulations with $\kappa T/L_D^2 = 6.95 \times 10^{-8}/M^2$. The prediction for γ_0 by the short wavelength mechanism

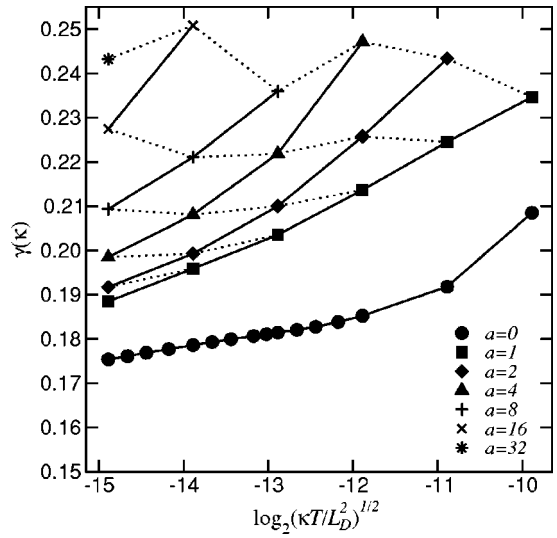

FIG. 7. Decay rate of scalar variance at different diffusivity κ and different amount (controlled by a) of long wavelength damping. The dotted lines connect data points with the same ak_0/k_d ratio.

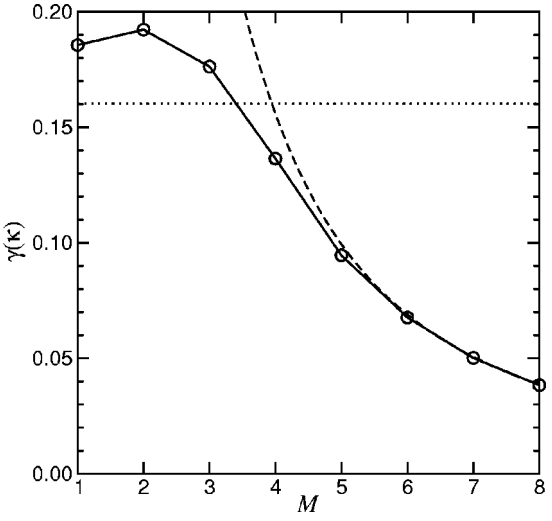

FIG. 8. Decay rate of scalar variance as a function of M where $M=L_D/L_f$ (circle). The dotted line is the prediction for γ_0 by the short wavelength mechanism and the dashed line is the long wavelength mechanism upper bound Eq. (48).

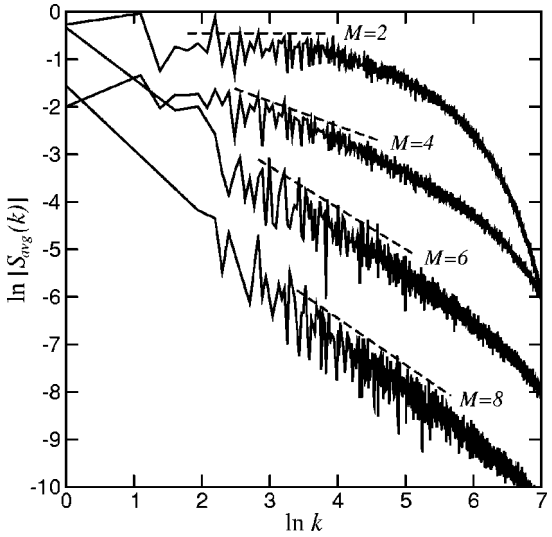

FIG. 9. Averaged wave number power spectra $S_{\mathrm{avg}}(k)$ for different values of M (Fourier modes with zero amplitude are omitted). The dashed lines are the linear fits used to estimate the scaling exponents ψ.

(dotted line) and the long wavelength mechanism upper bound Eq. (48) (dashed line) are also shown. $\gamma(\kappa)$ remains roughly constant for small M, and then decreases as M increases for $M>3$. This result is in agreement with Eq. (51). We interpret the fact that $\gamma(\kappa)$ at $M=1,2,3$ exceeds the $\kappa=0$ short wavelength mechanism upper bound as being due to finite diffusion (e.g., see inset to Fig. 4).

The upper bound Eq. (48) is obtained by removing all the variance "leaking out" from the longest wavelength Fourier mode. As can be seen in Fig. 8, for $M>3$, the upper bound Eq. (48) is smaller than the short wavelength mechanism prediction Eq. (12). Thus, the excellent agreement between the numerical results and the dashed line in Fig. 8 shows that the variance decay rate is indeed determined by the processes at the longest wavelength for large M. Our numerical results also support the statement made in Sec. III C that as $M\rightarrow\infty$, Eq. (48) approaches the true value of γ_0. On the other hand, for $M\leqslant 3$, Fig. 8 shows that the decay rates obtained from our numerical experiments remain close to the value predicted by Eq. (12).

As discussed in Sec. II, the long wavelength mechanism is associated with a power-law wave number power spectrum. Figure 9 shows the time-averaged power spectrum $S_{\mathrm{avg}}(k)$, defined in Eq. (53), for different values of M. As expected, for large M, the spectrum decreases with increasing k as a power law $S_{\mathrm{avg}}(k)\sim k^{-\psi}$, while for small M, $S_{\mathrm{avg}}(k)$ has similar shape as the spectrum shown in Fig. 5 for the case $L_D=L_f$. For $\psi>0$, the Lagrangian stretching theory gives the relation Eq. (31) between ψ and γ_0. Using the technique described in Sec. II C, in particular Eq. (35), we can evaluate ψ theoretically as a function of γ_0. The result is shown as dashed line in Fig. 10. The value of ψ drops from 1 to 0 as γ_0 increases from 0 to the value given by Eq. (12). We also measure the exponent ψ of our numerically obtained power spectrum $S_{\mathrm{avg}}(k)$ for different values of M. The results are plotted against the corresponding measured $\gamma(\kappa)$ as circles in Fig. 10. The numerical results agree fairly well with the theory. The discrepancy is probably due to the small but nonzero value of κ used in the numerical experiments.

V. CONCLUSION

We consider the advection of passive scalars in chaotic fluid flows. Two mechanisms that lead to a positive exponential damping rate γ_0 of scalar variance in the zero diffusivity limit are studied: (i) the short wavelength mechanism which is based on Lagrangian stretching theory and (ii) the long wavelength mechanism which involves processes taking place at the longest length scale of the system.

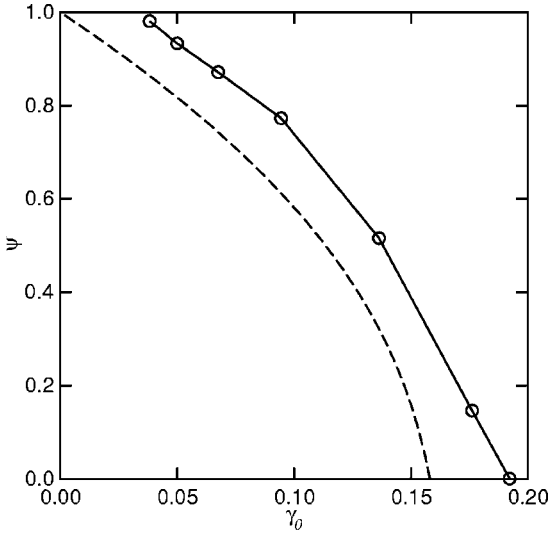

FIG. 10. Wave number power spectrum scaling exponent ψ versus scalar decay rate γ_0. The dashed line is the theoretical result obtained by Eq. (31). Circles are results from numerical experiments using small but finite κ.

Subject to the satisfaction of hypothesis Eq. (27), the damping rate predicted by the short wavelength mechanism Eq. (12) gives an upper bound for γ_0. For the particular flow [Eqs. (36)–(39)] that we study, we find that, when the system length scale L_D is comparable to the length scale of the flow L_f, our numerical experiments (which employ gird size up to 6×10^4 by 6×10^4) provide strong evidence that the short wavelength mechanism applies and γ_0 is given by Eq. (12). On the other hand, when $L_D \gg L_f$, the long wavelength mechanism applies. For the flow we study, we obtain a sufficient condition Eq. (51) for the applicability of the long wavelength mechanism.

The two mechanisms can be distinguished, possibly experimentally, by measuring the wave number power spectrum. For small diffusivity, the long wavelength mechanism produces a spectrum that decreases as a power law, while the short wavelength mechanism produces a spectrum that is flat out to the diffusive cutoff scale.

Finally we note that we have very recently received a preprint of a paper by P. H. Haynes and J. Vanneste [25] which also treats the regimes of applicability of the short and long wavelength mechanisms of passive scalar decay.

ACKNOWLEDGMENTS

We have benefited from correspondence with Peter H. Haynes and from access to a preprint of work by D. R. Fereday and P. H. Haynes [15]. This work was supported by the U.S. Office of Naval Research (Physics).

APPENDIX: NUMERICAL TECHNIQUE

The version of the lattice technique [1,5] used in Sec. IV is as follows. Let $\phi_n^{(p,q)}$ denote the scalar field value at the grid point $(x,y)=(p\Delta,q\Delta)$, where p and q are integers, Δ is the grid spacing, and the scalar field is evaluated just after the nT smoothing step (Sec. IV). Now we perform the advection step to obtain $\phi_{n+(1/2)}^{(p,q)}$ by (i) using the map Eq. (40) to take the grid point $x=p\Delta$, $y=q\Delta$ backward in time to a point (x',y') and (ii) linearly interpolating the ϕ_n from the four grid points nearest (x',y') onto (x',y'). Referring to Fig. 11,

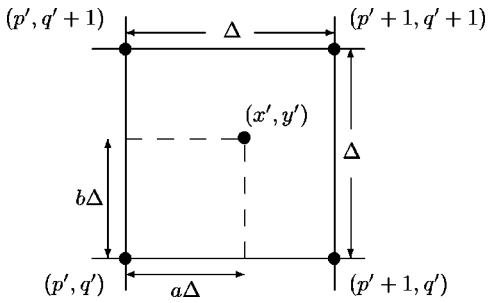

FIG. 11. Illustration of interpolation in the advection step. a and b are in (0,1).

$$\phi_{n+1/2}^{(p,q)} = (1-a)(1-b)\phi_n^{(p',q')} + a(1-b)\phi_n^{(p'+1,q')} + (1-a)b\phi_n^{(p',q'+1)} + ab\phi_n^{(p'+1,q'+1)}. \tag{A1}$$

This interpolation contributes an amount of large scale diffusion equal to $\kappa_i=\Delta^2/(6T)$. (Here by "large scale" diffusion we mean that for variation of ϕ over a scale much larger than Δ, the interpolation acts approximately the same as would diffusion of size κ_i.) We next do an additional smoothing of $\phi_{n+(1/2)}^{(p,q)}$ to obtain $\phi_{n+1}^{(p,q)}$

$$\phi_{n+1}^{(p,q)} = \sum_{|r|,|s|\leqslant 2} C_{|r|}C_{|s|}\phi_{n+1/2}^{(p+r,q+s)}, \tag{A2}$$

where we have chosen smoothing coefficients $C_0=1/8$, $C_1=1/4$, and $C_2=3/16$. This gives an additional smoothing contribution to the large scale diffusion of $\kappa_s=\Delta^2/T$, so that the total diffusion is $\kappa=\kappa_i+\kappa_s=(7/6)\Delta^2/T$. The particular choice we use for the constants, C_0, C_1, and C_2, has the property that the smoothing step Eq. (A2) takes the coefficient of the highest allowed Fourier components on the grid (i.e., $\exp[i\pi x/\Delta]$ and $\exp[i\pi y/\Delta]$) exactly to zero.

Note that for the advection step Eq. (A1) [and the smoothing step Eq. (A2)] the computation of the values of $\phi_{n+1/2}^{(p,q)}(\phi_{n+1}^{(p,q)})$ at grid point (p,q) depends only on values $\phi_n^{(p',q')}(\phi_{n+1/2}^{(p',q')})$ at the previous half step, and is therefore independent of current values on other grid points. Thus these computations can be done in parallel, and can be very fast.

[1] R. T. Pierrehumbert, Chaos, Solitons Fractals **4**, 1091 (1994).
[2] T. M. Antonsen, Jr., Z. Fan, E. Ott, and E. Garcia-Lopez, Phys. Fluids **8**, 3094 (1996).
[3] D. T. Son, Phys. Rev. E **59**, R3811 (1999).
[4] E. Balkovsky and A. Fouxon, Phys. Rev. E **60**, 4164 (1999).
[5] R. T. Pierrehumbert, Chaos **10**, 61 (1999).
[6] D. R. Fereday, P. H. Haynes, A. Wonhas, and J. C. Vassilicos, Phys. Rev. E **65**, 035301 (2002).
[7] A. Wonhas and J. C. Vassilicos, Phys. Rev. E **66**, 051205 (2002).
[8] J. Sukhatme and R. T. Pierrehumbert, Phys. Rev. E **66**, 056302 (2002).
[9] A. Pikovsky and O. Popovych, Europhys. Lett. **61**, 625 (2003).
[10] M. Chertkov and V. Lebedev, Phys. Rev. Lett. **90**, 034501 (2003). The wall induced damping mechanism discussed here may be relevant in many typical situations.
[11] G. A. Voth, T. C. Saint, G. Dobler, and J. P. Gollub, Phys. Fluids **15**, 2560 (2003).
[12] J.-L. Thiffeault, and S. Childress, Chaos **13**, 502 (2003).
[13] J.-L. Thiffeault, Chaos **14**, 531 (2004).
[14] W. Liu and G. Haller, Physica D **188**, 1 (2004).
[15] D. R. Fereday and P. H. Haynes, Phys. Fluids **16**, 4359 (2004) .

[16] T. M. Antonsen, Jr., Z. Fan, and E. Ott, Phys. Rev. Lett. **75**, 1751 (1995).
[17] R. S. Ellis, *Entropy, Large Deviations and Statistical Mechanics* (Springer-Verlag, New York, 1985).
[18] E. Ott and T. M. Antonsen, Jr., Phys. Rev. Lett. **61**, 2839 (1988).
[19] F. Varosi, T. M. Antonsen, Jr., and E. Ott, Phys. Fluids A **3**, 1017 (1991).
[20] E. Ott, *Chaos in Dynamical Systems*, 2nd ed. (Cambridge University Press, Cambridge, 2002).
[21] A. A. Schekocihin, P. H. Haynes, and S. C. Cowley, Phys. Rev. E **70**, 046304 (2004).
[22] C. Reyl, T. M. Antonsen, Jr., and E. Ott, Phys. Plasmas **5**, 151 (1998).
[23] C. Reyl, T. M. Antonsen, Jr., and E. Ott, Phys. Rev. Lett. **78**, 2559 (1997); "Physica D **111**, 202 (1998).
[24] Y.-K. Tsang, E. Ott, and T. M. Antonsen, Jr., e-print cond-mat/0503424, Phys. Rev. E (to be published).
[25] P. H. Haynes, and J. Vanneste, "What controls the decay of passive scalars in smooth flows?," Phys. Fluids (to be published).